The Wall-PIV Measurement Technique for Near Wall Flow Fields in Biofluid Mechanics

André Berthe, Daniel Kondermann, Christoph Garbe, Klaus Affeld, Bernd Jähne, and Ulrich Kertzscher

Abstract. This chapter describes the development of a new time resolved 3D PIV technique for near wall flow field measurements. This measurement technique, called wall-PIV, is based on Beer-Lambert's law. It substitutes the classical PIV laser sheet by a diffuse, monochromatic full-field illumination that is limited to the near wall region by an absorbing molecular dye in the fluid. Aimed range of applications is the investigation of flow fields next to one- or two dimensionally curved, possibly flexing surfaces. The three dimensional three component flow estimation uses a new optical flow algorithm, based on particle trajectories. Results of the measurement technique's application on a displacement pediatric blood pump are presented.

1 Introduction

The time resolved measurement of three dimensional flow fields next to non-plane surfaces is of great interest in biofluid mechanics. Many medical issues, such as thrombotic events and atherosclerosis, depend on shear stresses and shear rates near vaulted walls [18]. Hereby we define a vaulted wall as a wall with two main non-zero curvatures. The investigation of flow fields and shear stresses near vaulted walls is non-trivial. Moreover, biological surfaces and some parts of artificial organs are often moving. Among others, the development of the wall-PIV technique aims for the full-field investigation of shear stresses at membranes of displacement pumps. The movement of the membranes with up to 2 Hz requires the application of a measurement technique that can capture instantaneously and non-contacting the flow field

André Berthe · Klaus Affeld · Ulrich Kertzscher
Biofluid Mechanics Laboratory, Charité - Universitätsmedizin Berlin,
Thielallee 73, D-14195 Berlin
andre.berthe@charite.de

Daniel Kondermann · Christoph Garbe · Bernd Jähne
Digital Image Processing Research Group, Heidelberg Collaboratory for Image Processing,
University of Heidelberg, Speyerer Straße 4, D-69115 Heidelberg
daniel.kondermann@iwr.uni-heidelberg.de

W. Nitsche and C. Dobriloff (Eds.): Imaging Measurement Methods, NNFM 106, pp. 11–20.
springerlink.com

in the near wall region. Thereby many well established point and field measurement techniques are of limited use. Today, there are several 3D measurement techniques and shear stress measurement techniques. A brief overview of them is given in section 2. Then, in section 3 the measurement technique including the used algorithm of flow estimation is described. Following, section 4 shows an error estimation for this approach. To distinguish between aberrations of measurements and aberrations of the flow estimation, artificial data sets and experiments with known analytical solution and known particle position, called "single particle experiments" were established (see section 5). Concluding, section 6 shows results of an experiment on a pediatric blood pump.

2 Flow and Shear Stress Measurement Techniques

Some medical measurement techniques as magnetic resonance imaging (MRI) and echocardiography allow the three dimensional measurement of flow fields. However, their spatial and temporal resolutions are not yet sufficient for the investigation of near wall flow fields. First tests to access near wall flows and wall shear stresses using MRI showed clearly the current limitations of this technique [19].

In the following we will only consider field methods, that can measure instantaneously a whole flow field. Most of these techniques are reviewed in [6, 17]. However, only few of them have the potential to be used at vaulted walls. The most promising techniques for the instantaneous, time resolved measurement of three dimensional flow fields are based on PIV.

Holographic PIV seems to provide a high potential for the assessment of near wall flows. This technique is based on a hologram, storing particle positions obtained from the interference pattern of a reference light beam and reflected light of the recorded particles. Reference beam and scattered light have to be recorded at a small angle, so that numerical aperture and depth resolution are limited [11]. Furthermore, until now high resolutions urge the use of holographic films what leads to huge processing times. The development of measurement and computer hardware might enhance the potential and solve the limitations of this technique in the future.

Defocusing digital PIV (DDPIV) and 3D PTV are based on particle identification on recordings of multiple directions. Limitations of these techniques are given by the alignment of the optical axes and the particle density. According to Hill et al. (2008) the seeding density of DDPIV can be higher than in PTV [10]. Inherent limitation of the setup, sold by TSI Inc. (Shoreview, USA) as "Volumetric 3-component velocimetry", is the direct transfer of the camera's alignment to the particle's alignment. This requires a plane flow phantom surface, aligned normal to the camera-setups center-line. Providing these conditions, the technique should be tested for a part of the described applications in biofluid mechanics.

Tomographic PIV uses the same camera setup with an expanded laser sheet and typically four cameras. According to Elsinga et al. (2006) the technique allows approximately 10 times higher particle densities than 3D PTV. This results from the fact, that the technique does not identify single particles. Instead, a three dimensional

light intensity distribution is reconstructed by a tomography algorithm and a 3D cross-correlation is applied on the voxels of the reconstructed volume [6]. A new challenge of this approach is the appearance of so called "ghost-particles". This kind of errors depends strongly on the number of cameras and the particle diameter (see [22] for details). A further problem of this technique are high processing times of about thirty minutes to one hour for one volume (see [24, 1]).

3 Wall-PIV

The measurement principle of wall-PIV is similar to that of PIV: The displacement of tracer particles in an illuminated thin region of the fluid is recorded. Subsequently the velocity of the fluid is estimated by, depending on the flow estimation algorithm, the displacement of particles (particle tracking), the displacement of speckles (cross-correlation) or the displacement of image gray values (optical flow). In PIV the classical algorithm is cross-correlation, allowing higher particle densities than PTV. The application of optical flow algorithms is relatively new to PIV. For wall-PIV all three kinds of algorithms have been tested (see subsection 3.2).

3.1 Wall-PIV Setup

The major difference between PIV and wall-PIV is the kind of illumination: In most PIV setups (ignoring e.g. micro-PIV), the flow is illuminated by a laser sheet. The thickness of this light sheet for applications with cross-sections of several tenths of millimeters is approximately 0.5 to 1.0 mm. As a light sheet can not be aligned to a vaulted surface, the transparent flow phantom is fully illuminated from the outside with a diffuse monochromatic light placed next to the camera. To limit the depth of view of particles to approximately 0.3 mm, a molecular dye with a high absorbance for the immited wavelength of light is added to the fluid, a further key difference from PIV. The depth of light penetration and thereby the depth of view can be adjusted by varying either the incoming light intensity or the concentration of the dye.

When monochromatic light with the light intensity I_0 penetrates a fluid, the intensity will be decreased by absorption on the way through the fluid (see sketch of Fig. 1). Assuming an incidence of light at a particle at a distance R from the surface of the wall, the reduced light intensity is given by I_p, which can be calculated with the Beer-Lambert's law (1).

$$I_p = I_0 \cdot \exp(-\varepsilon \cdot c \cdot R) \tag{1}$$

In equation 1, ε is the molar absorption coefficient of the dyed fluid and c is the concentration of the dye.

Assuming total reflection of the light on the particle, the reflected light passes the same distance R through the fluid again. The intensity is reduced to the intensity I, given by equation (2).

$$I = I_p \cdot \exp(-\varepsilon \cdot c \cdot R) = I_0 \cdot \exp(-2 \cdot \varepsilon \cdot c \cdot R) \tag{2}$$

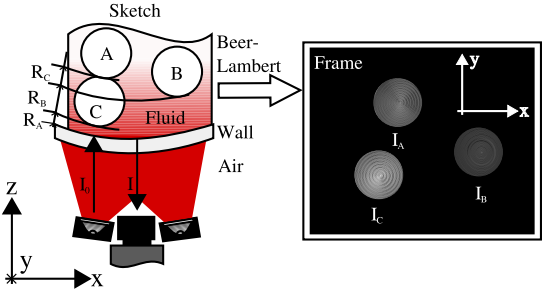

Fig. 1 Illustration of the method used in wall-PIV: On the left a sketch of part of the fluid flow and the apparatus used. It shows the illuminated region of the fluid and three tracer particles A, B and C with the corresponding distances R. On the right a representation of an image recorded by the camera with the corresponding particle intensities I_A, I_B, and I_C

Neglecting the absorption of light by the transparent flow phantom and the exterior air, the gray value, recorded by the camera is proportional to the light intensity I. Thereby, it is possible to use the recorded gray value of the particle as depth information. Including the gray values and the displacement of a recorded particle, we obtain principally all three components and all three coordinates. In section 4 the causes of variations between theoretical and recorded values, as well as the resulting calibration techniques are discussed.

3.2 Flow Estimation Algorithm

A straightforward approach to obtain a 3D near wall flow field by the gray values of recorded particles is their separation in several layers. Following, a 3D-2C flow field can be calculated by a cross-correlation for every layer [4]. However, the image data contains enough information to calculate the whole 3D-3C flow field.

In the field of optical flow (OF) estimation, techniques based on the Brightness Constancy Constrained Equation (BCCE) assume that a pixel intensity remains constant along its trajectory of motion:

$$(I(x,y,t) - I(x,y,t+1))^2 = 0 \tag{3}$$

This quadratic penalization of the discrepancy of this model is then linearized by first order Taylor Expansion, yielding the traditional BCCE:

$$\mathbf{d}^\top \mathbf{p} = [I_x, I_y, I_t] \cdot [u_1, u_2, 1]^\top = 0. \tag{4}$$

Partial derivatives are denoted by subscripts, I is the image and (u_1, u_2) the flow to be estimated. Basic methods using this constraint have been proposed in local [21] and global [12] optimization frameworks. A more recent application of OF in the PIV community is e.g. [23]. Whenever particles are large and slow and/or dense

enough, such BCCE-based flow estimation techniques can be applied (for details see e.g. [23]).

To adapt the standard BCCE to our needs, we made use of its extension proposed in [9], which incorporates models of brightness changes to obtain the so-called Brightness Change Constrained Equation for exponential decay:

$$\mathbf{d}^\top \mathbf{p} = [\kappa, I_x, I_y, I_t] \cdot [I, u_1, u_2, 1]^\top = 0. \tag{5}$$

The additional unknown κ is the constant of exponential decay and thus directly related to the depth of the particle image through Beer-Lambert's law. As described above, the flows measured by our method are two dimensional projections of inherently three dimensional flows. Hence, spatial motion models can not assist in the finding of correct motion estimates. Global techniques make assumption of spatial motion models by means of regularization, rendering these approaches infeasible for our needs. Therefore we limited ourselves to the study of local approaches.

To this end, we developed a method to deal with our new BCCE [14, 15]. Together with advanced preprocessing techniques [14] this method can be used to directly measure wall shear rates from wall-PIV images.

The faster the motion of particles, the more difficult the estimation of the flow of the particle images by OF algorithms becomes and conventional OF techniques fail. Furthermore, the computation of image derivative approximations can not easily be estimated for small particle images. Therefore, we firstly did not linearize the BCCE as in equation 4. Secondly, instead of formulating a spatial motion model, we formulated a purely temporal motion model based on trajectories by means of unsupervised learning techniques as detailed in [20]. As the used trajectories are only of limited length (between 5 and 19 time steps), the trained model is on the one hand sufficient to represent a large number of flows, which have not yet been observed but on the other hand captures important properties of the training data. Hence, the trajectory motion model alleviates the nonlinear optimization by limiting the search space to a statistically meaningful subset of all possible motions.

4 Error Estimation

First of all, the particles ability to follow the flow has to be investigated. One practicable approach is the calculation of the Stokes number, that should be much smaller than 1. Calculations based on the definition of Subramanian and Brady (2006) complied with this criterion for investigated flows [25].

In wall-PIV the depth position of a tracer particle, moving with its center of mass, is obtained from the reflection on its surface. This has to be included by adding the particle's radius to the distance of its surface to the wall. Consequently, variations of the particle's diameter lead to falsified shear rates. The relative error of shear rate calculations is given in [2].

In section 3.1 a total reflection of light at the tracer particle was assumed. For the used wavelength silver has a reflectance r of about 0.9. Introducing this into the calculation of the particle distance R from equation 2, we obtain equation 6:

$$R = \frac{-1}{2 \cdot \varepsilon \cdot c} \cdot \ln(r \cdot \frac{I}{I_0}) = \frac{-1}{2 \cdot \varepsilon \cdot c} \cdot (\ln(\frac{I}{I_0}) + \ln(r)) \tag{6}$$

We can conclude, that the partial reflectance would lead to a fix offset for all depth estimates. The same would result from a faulty value for the incoming light intensity I_0. Calibrating the measurement technique with a particle at depth zero and compensating light fluctuations based on a calibration target incorporated in the image sequences can cancel out this source of aberrations. In cases where the intensity I_0 can not be assumed constant over the whole ROI or can not be accessed in the flow phantom, two monochromatic wavelength λ_1 and λ_2 can be used instead of one. This bi-chromatic approach allows the reference to the ratio $\frac{I_{0,1}}{I_{0,2}}$ instead of a reference to the absolute values [15]. When using flow phantoms from materials with non-selective absorbance, the ratio, and thereby the used reference value, is not changed by different material thickness.

Uncertainties in particle depth caused by sensor noise are proportional to the uncertainty of the recorded gray value. The resulting resolution of depth of wall-PIV can be estimated with 60 layers for a 8 bit camera with 5 % signal to noise ratio [15].

5 Experimental Validation

Experimental validation of a flow measurement technique requires the exact knowledge of a flow under investigation. Exact analytical solutions of the Navier Stokes equations are rare [13]. The wall-PIV technique was first validated on a rectangular duct [4], showing a good agreement between theoretical and experimental data. Another validation was realized on a falling film, providing reliable depth estimations for the near wall region as well [15]. However, both investigated flows did not provide a proof for the ability to measure all three components of the flow. Exact analytical solutions for a fully 3D-3C flow exist, but are unfortunately not applicable experimentally [7]. Therefore no such solutions can be used to gain insight in the quality of wall-PIV as 3D-3C measurement technique. Experiments on a u-shaped duct with backward facing step compared wall-PIV results to classical PIV and computational fluid dynamics [4, 16]. However, aberrations between the resulting flow fields can not be easily assigned to a source of aberration. To overcome this limitation, artificial traversals of particles have been used. The basic idea of a particle traversal is to realize a known particle movement under realistic measurement conditions. The depth traversal of several particles on a glass support showed good results for the wall-PIV technique's depth measurement abilities under two different hardware configurations [4, 15]. The depth resolution of this approach is limited due to its mechanical accuracy (the support has to stay exactly plane-parallel to the wall) and adhesive forces can occur between the supporting media and the wall. Therefore the technique was developed to "single particle setups" for further calibrations and multi-directional movements [3]. In a single particle setup, one particle is attached to a glass capillary. The diameter of the capillary is inferior to that of the particle,

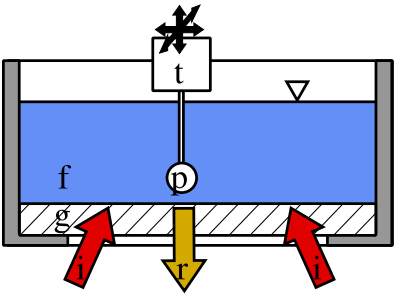

Fig. 2 Detail of the single particle setup: The particle p is connected by the capillary at the milling cutter, representing a three dimensional traversal system t. Immited light i enters the reservoir filled by the bottom through a glass window g. After transversal of the fluid f the reflected light r is captured by a camera

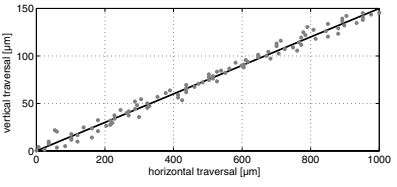

Fig. 3 Flow estimation on a horizontally and vertically traversed particle. Markers show the estimated flow, the solid line shows the particle traversal.

so that the support is hidden from the bottom. Attaching the capillary at a traverse system, the particle can be moved three dimensionally with the given accuracy of the system. For the presented experiments we used a high precision milling cutter (at the Fachgebiet Micro- und Feingerätetechnik, TU Berlin), allowing a traversal accuracy up to 100 nm in all three directions. A systematic sketch of the setup is shown in Fig. 2. Further details of the setup are given in [3]. Figure 3 shows a flow estimation on a horizontally and vertically traversed particle. As flow estimation algorithm we used the trajectory approach of section 3.2. The horizontal traversal was of 1000 μm, the vertical traversal was of 150 μm. The average error for the horizontal movement was 0.0453 px with a standard deviation of 0.0359 px.

6 Experiments

The flow at the back of a pediatric displacement blood pump model with a stroke volume of 10 ml was investigated. Optical diffractions at the inner surface of the pump were avoided by a replacement of the polyurethane pump wall by a silicone block with identical refractive index as the used test fluid. The inner shape of the silicone block was identical to that of the original wall, the outer wall of the transparent silicone was plane. To avoid mechanical deformation, the silicon was surrounded by a glass housing.

The inflow of the pump was connected to a reservoir of a size of 250 mm x 250 mm, so that the change in the fluid level during the pumping caused a negligible pressure variation of less than 1 %. The outflow was connected to a windkessel (see Fig. 4), allowing the adjustment of the pressure curve to biological conditions.

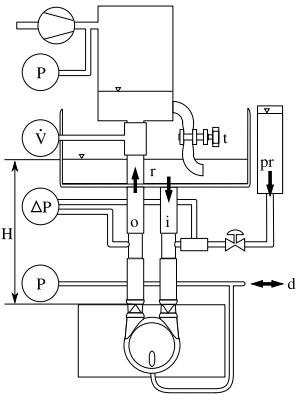

Fig. 4 Mock circulation used during the investigation of a displacement pump. Pressure variations at the inflow *i* were below 1 % because of the size of the reservoir *r*. Pressure measurements between inflow and outflow *o*, at the windkessel and at the drive line *d* as well as the flow rate at the outflow were registered by a data acquisition board. The windkessel was adjusted by the air pressure and a throttle *t*. Addition of particles can be effected by a particle reservoir *pr*

Pressure measurements at the windkessel were realized with a pressure sensor capable of measuring 0–300 mbar (SensorTechnics, Puchheim, Germany). The flow rate was measured using a ultrasonic flow meter T106 (Transonic Systems Inc., Ithaca, USA). A differential pressure sensor 24PC (Honeywell Inc., Minnesota, USA) was mounted between inflow and outflow duct. The displacement pump was actuated by a Linmot (NTI AG, Spreitenbach, Switzerland) driven pneumatic system. The systole (pump ejection phase) was set to 200 ms and the diastole (pump filling phase) to 300 ms.

Images were taken with 2080 frames per second (fps) with an image size of 1280x1048 pixels with a Redlake MotionPro X-3 (Imaging Solutions GmbH, Eningen, Deutschland). A fixed focal lens of 50 mm, 1:0.95 was used at f 2.8.

Illumination was realized with two light panels. Each of them assembling 104 3 W Luxeon LED (Philips Lumileds, San Jose, USA); 48 with a wavelength of $\lambda_1 = 617$ nm and 56 with a wavelength of $\lambda_2 = 627$ nm. By a trigger impulse the illumination changed between both wavelengths.

Camera, light sources, pneumatic system and sampling rate of the sensors (10 data points per image) were triggered by a PCI 1200 data acquisition board (National Instruments, Austin, USA). The same board was used to acquire the sensor data sets. LabView 8.0 (National Instruments, Austin, USA) was used for system control and data acquisition.

We used silver coated hollow ceramic spheres with a diameter of 71 to 75 μm (Potters Industries Inc., Carlstadt, USA).

The used fluid was a mixture of distilled water and glycerin with 37.5 vol-% glycerin (CVH, Hannover, Germany) with a viscosity of 3.5 mm^2/s . The viscosity corresponds to that of blood with determined viscosities between 2.5 mm^2/s to 5.6 mm^2/s (see [5, 8] for the viscosity of blood).

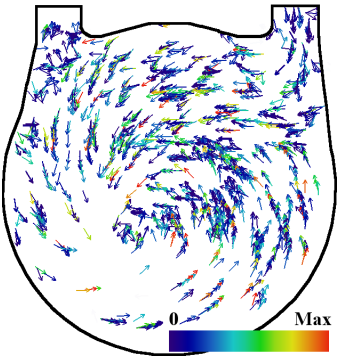

Fig. 5 Velocity field estimate for the pediatric blood pump with a stroke volume of 10 ml. The motion vectors indicated direction of the flow, whereas color denotes vector magnitude. Please note that the mixture of long and short vectors is due to particle images moving in different depths of the projected real volume, showing that spatial regularization techniques of standard OF algorithms would fail in this context

The fluid was dyed with the food coloring dye patent blue V with a concentration of 0.3 mg/l. A phase averaged flow field over four pump cycles is shown in Fig. 5. The flow corresponds to the flow phase 0.025 s before start of the systole (ejection phase). We can see, that a vortex fills the whole pump body, providing a good wash out of the pump. Colors of the vectors indicate different vector magnitudes, coupled to different particle depth. The presented data provides a starting point for the calculation of wall shear stresses.

Acknowledgements. We gratefully acknowledge the support of the Deutsche Forschungsgemeinschaft DFG within the research program SPP 1147. We also thank the MFG, TU Berlin for their support.

References

1. Atkinson, C.H., Dillon-Gibbons, C.J., Herpin, S., Soria, J.: Reconstruction techniques for tomographic piv (tomo-piv) of a turbulent boundary layer. In: Proceedings of the 14th International Symposium on Applications of Laser Techniques to Fluid Mechanics, Lisbon, Portugal (2008)
2. Berthe, A., Christensen, C., Debaene, P., Goubergrits, L., Kertzscher, U., Affeld, K.: Further development of an image-based optical measurement technique for complex near-wall flows. In: The 12th International Symposium on Flow Visualization, Goettingen, Germany (2006)
3. Berthe, A., Kondermann, D., Christensen, C., Goubergrits, L., Kertzscher, U.: Using single particles for the validation of a 3d-3c near wall measurement technique. In: The 7th International Symposium Particle Image Velocimetry, Rome, Italy (2007)
4. Debaene, P., Kertzscher, U., Goubergrits, L., Affeld, K.: Visualization of a wall shear flow: Development of a new particle image interrogation method. J. Visual-Japan 8, 285–364 (2005)
5. Dintenfass, L.: Blood Microrheology – Viscosity Factors in Blood Flow, Ischaemia and Thrombosis. Butterworths, London (1971)

6. Elsinga, G., Scarano, F., Wieneke, B., van Oudheusden, B.: Tomographic particle image velocimetry. Experiments in Fluids 41(6), 933–947 (2006)
7. Ethier, C.R., Steinman, D.A.: Exact fully 3D navier-stokes solutions for benchmarking. International Journal for Numerical Methods in Fluids 19(5), 369–375 (1994)
8. Geigy, J. (ed.): Documenta Geigy, Wissenschaftliche Tabellen, 6th edn. Geigy (1960)
9. Haussecker, H., Fleet, D.: Computing optical flow with physical models of brightness variation. IEEE Transactions on Pattern Analysis and Machine Intelligence (PAMI) 23(6), 661–673 (2001)
10. Hill, D., Troolin, D., Walters, G., Lai, W., Sharp, K.: Volumetric 3-component velocimetry (v3v) measurements of the turbulent flow in stirred tank reactors. In: Proceedings of the 14th International Symposium on Applications of Laser Techniques to Fluid Mechanics, Lisbon, Portugal (2008)
11. Hinsch, K.D.: Holographic particle image velocimetry. Measurement Science and Technology 13(7), R61–R72 (2002)
12. Horn, B., Schunck, B.: Determining optical flow. Artificial Intelligence 17, 185–204 (1981)
13. Hui, W.H.: Exact solutions of the unsteady two-dimensional navier-stokes equations. Zeitschrift für Angewandte Mathematik und Physik (ZAMP) 38(5), 689–702 (1987)
14. Jehle, M.: Spatio-temporal analysis of flows close to free water surfaces. PhD thesis, University of Heidelberg (2006)
15. Jehle, M., Jähne, B.: A novel method for three-dimensional three-component analysis of flows close to free water surfaces. Experiments in Fluids 44(3), 469–480 (2008)
16. Jehle, M., Jähne, B., Kertzscher, U.: Direct estimation of the wall shear rate using parametric motion models in 3D. Pattern Recognition, 434–443 (2006)
17. Kertzscher, U., Debaene, P., Goubergrits, L., Affeld, K.: Experimental assessment of wall shear flow. In: Kowalewski, T. (ed.) Abiomed Lecture Notes: Blood Flow, Modelling and Diagnostics, 6, Abiomed, Warschau, pp. 109–134 (2005)
18. Kertzscher, U., Berthe, A., Goubergrits, L., Affeld, K.: Particle image velocimetry of a flow at a vaulted wall. Proceedings of the Institution of Mechanical Engineers, Part H: Journal of Engineering in Medicine 222(4), 465–473 (2008)
19. Köhler, U., Marshall, I., Robertson, M.B., Long, Q., Xu, X.Y., Hoskins, P.R.: Mri measurement of wall shear stress vectors in bifurcation models and comparison with cfd predictions. Journal of Magnetic Resonance Imaging 14(5), 563–573 (2001)
20. Kondermann, D., Kondermann, C., Berthe, A., Kertzscher, U., Garbe, C.: Motion estimation based on a temporal model of fluid flows. In: The 13th International Symposium on Flow Visualization, Nice, France (2008)
21. Lucas, B., Kanade, T.: An iterative image registration technique with an application to stereo vision (darpa). In: Proceedings of the 1981 DARPA Image Understanding Workshop, pp. 121–130 (1981)
22. Michaelis, D., Wieneke, B.: Comparison between tomographic piv and stereo piv. In: Proceedings of the 14th International Symposium on Applications of Laser Techniques to Fluid Mechanics, Lisbon, Portugal (2008)
23. Ruhnau, P., Schnörr, C.: Optical stokes flow estimation: an imaging-based control approach. Experiments in Fluids 42(1), 61–78 (2007)
24. Schroeder, A., Geisler, R., Elsinga, G., Scarano, F., Dierksheide, U.: Investigation of a turbulent spot and a tripped turbulent boundary layer flow using time-resolved tomographic piv. Experiments in Fluids 44(2), 305–316 (2008)
25. Subramanian, G., Brady, J.F.: Trajectory analysis for non-brownian inertial suspensions in simple shear flow. Journal Of Fluid Mechanics 559, 151–203 (2006)